2024 IEEE International Conference on Robotics and Automation (ICRA 2024)
May 13-17, 2024. Yokohama, Japan

# A Hybrid Admittance Control Algorithm for Automatic Robotic Cranium-Milling

Chen Qian[1], Zhen Li[1], Qiang Ye[1], Peicong Ge[2], Jizong Zhao[2], and Gui-Bin Bian[1]

***Abstract*— Prior robot-assisted cranium-milling studies only considered controlling the force in the skull's vertical direction and neglected the milling cutter's feed force. Additionally, achieving stable force control in multiple directions is challenging for robots due to the uneven skull surface. Here a hybrid admittance control algorithm incorporating a model-free adaptive nonlinear force control and fuzzy control algorithms is proposed to accomplish effective automatic cranial-milling tasks. First, a pure data-driven model-free adaptive control method based on partial form dynamic linearization is used to control the feed force. Second, fuzzy control minimizes the total error of both the vertical and feed force by adaptively adjusting the milling cutter's velocity and position. 42 ex vivo animal skull-milling experiments conducted by the automatic robotic cranium-milling system indicate that when using the proposed control algorithm, the force error percentage can be maintained below 5.0% within 3 s and the maximal root mean square error percentages for vertical and feed force are 1.85% and 1.94%, respectively. Moreover, no instances of dura mater damage are observed and the robotic system exhibits a high level of autonomy as it performs the skull milling task with minimal human involvement throughout the entire experiment. The results suggest the potential for advancing the intelligence level of neurosurgery in the future.**

## I. INTRODUCTION

Craniotomy is the primary surgical procedure for treating brain tumors, utilizing mechanical devices to open the patient's cranium for intracranial surgery [1]. The surgical procedure typically involves three subtasks: Firstly, the scalp is removed to expose the skull, followed by drilling a hole using a craniotomy drill. Subsequently, a milling cutter is inserted into the hole to follow a predetermined path, eventually leading to the removal of the skull for subsequent surgical interventions. Finally, the skull is re-fixed to its original position [2]. The effectiveness of clinical craniotomy is typically assessed based on criteria such as positional accuracy, force control precision, dura mater protection success rate, and trajectory smoothness. In this automatic robotic cranium-milling work, the primary considerations are force control precision, dura mater protection success rate, and the autonomy of the robot.

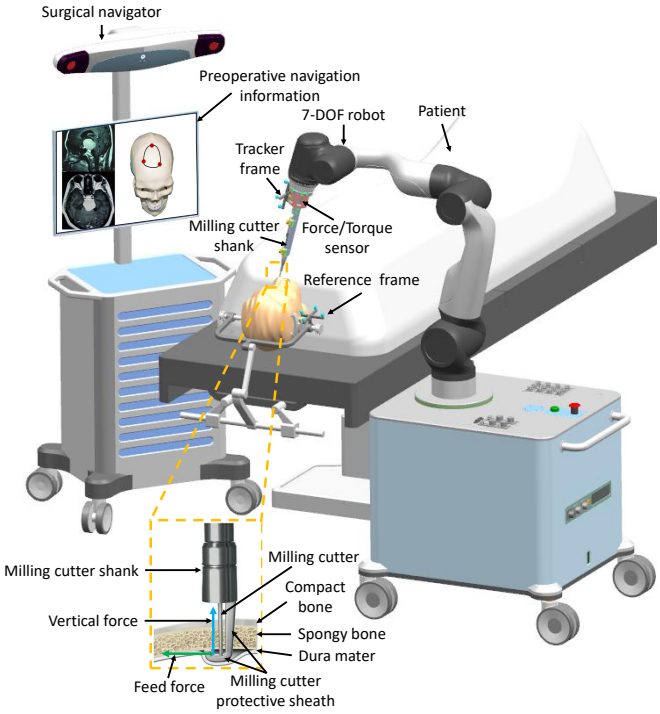


Fig. 1. Conceptual depiction of automatic robotic cranium milling. When integrated with preoperative diagnostic tools and surgical navigation systems, robotic technology holds the promise to eventually replace human surgeons in performing craniotomy procedures.

The skull is an intricate and layered structure that includes an inner dura mater layer, as shown in Fig. 1. The milling cutter is raised to make contact with the skull's lower surface using the milling cutter protective sheath to protect the dura mater during the cranium-milling procedure. Therefore, the milling cutter experiences both feed and vertical force during craniotomy. The main contributions are as follows:

1) A hybrid admittance control algorithm for cranium milling is designed. Adaptive nonlinear force control and fuzzy control are combined to control the feed and vertical force exerted on the skull within a certain range by adaptively adjusting the velocity and position of the milling cutter.

2) An automatic robotic cranium-milling method is proposed. The cranium-milling task can be automatically completed by utilizing a craniotomy robot system and incorporating force control methods based on predefined milling cutter movement direction and velocity.

3) 42 ex vivo skull-milling experiments are conducted on different animal skulls to validate the proposed algorithm.

This research is supported by the National Natural Science Foundation of China (Grant 62027813, U20A20196), the Beijing Science Fund for Distinguished Young Scholars (JQ21016), the Youth Innovation Promotion Association of the Chinese Academy of Sciences, Outstanding Member (Grant Y2022054), the EPSRC, Reference: EP/Y000773/1.

Corresponding author: Gui-Bin Bian

[1]Chen Qian, Zhen Li, Qiang Ye, and Gui-Bin Bian are with the Institute of Automation, Chinese Academy of Sciences, Beijing, 100190, China. (qianchen2021@ia.ac.cn, zhen.li@ia.ac.cn, qiang.ye@ia.ac.cn, guibin.bian@ia.ac.cn)

[2]Peicong Ge and Jizong Zhao are with the Beijing Tiantan Hospital, Capital Medical University, China National Clinical Research Center for Neurological Diseases, Beijing, 100050, China. (gepeicong@163.com, zhaojz205@163.com)

The result indicates that when using the proposed control algorithm, the force error percentage can be controlled below 5.0% within 3 s and the maximal root mean square error percentages for vertical and feed force are 1.85% and 1.94%.

The rest of the paper is organized as follows: Section II provides an overview of the advances in neurosurgical robots and force control methods for bone milling. Section III thoroughly describes the control method for skull milling. The experiments are presented in Section IV. The findings of the study are discussed in Section V. In Section VI, the conclusions of this study are summarized.

## II. RELATED WORK

Several robot-assisted systems have been developed for neurosurgery, such as NeuroMate and RoboDoc. However, these systems have constraints regarding flexibility, precision, expense, and controlling milling cutter vibration [3]. To tackle these challenges, innovative robotic systems for craniotomy have been developed. Johns Hopkins University has integrated commercial products, including a 3D Slicer, Stealthstation navigation system, NeuroMate surgical manipulator, six-dimensional force sensor, and application controller, to construct a robot system for craniotomy [4]. This system offers good mechanical stability, accuracy, and flexible workspace. However, it is bulky and obtrusive in the operating room and limited to 5 degrees of freedom (DOF). NeuroArm [5] is an integrated surgical system with image navigation designed for neurosurgery by the University of Calgary in Canada. The system includes three robotic manipulators, consisting of two 6-DOF master manipulators, a virtual reality display, and specialized surgical instruments. However, there remains room for improvement in terms of position precision.

Force control is vital for preventing damage to normal bone tissue caused by milling cutter vibrations during bone milling. However, due to system complexity and parameter uncertainties, force control is challenging. Some researchers have designed force control methods to address this problem. Xu [6] used motion constraints and safety equidistant surfaces to conduct beagle skull model milling experiments. However, they focused on vertical force control and neglected the milling cutter's feed force. Deng [7] designed a fuzzy force control system that adjusted the parameters to mill the intricate anatomical structure of the lamina. The force controller incorporated a fuzzy combiner, allowing it to adjust its control parameters in real-time. However, this method neglected the dynamic properties of the robot, resulting in large errors in force tracking. Wu [8] proposed a force prediction model constructed using the least squares multiple regression algorithm. However, the deviation between actual force and predicted force exceeded 0.5 N. Al-Abdullah [9] used the artificial neural network method to construct suitable models for force and temperature based on data gathered from experiments involving bone grinding on synthetic cancellous bone tissue. However, obtaining precise contact force through a mathematical model during skull milling is challenging due to uncertainties, such as collisions.

## III. METHOD

### A. Force Control in Feed Direction

According to [10], the feed force is related to the milling cutter's feed velocity $v_{feed}$, spindle speed $v_{spindle}$, structural characteristics, and the bone's thickness. The spindle speed remains constant during craniotomy surgery, and the structural characteristics of the milling cutter are unchanging. Consequently, the skull's thickness and the milling cutter's feed velocity primarily influence the feed force, leading to fluctuations during the saturation phase. Nevertheless, excessive fluctuations of the feed force can cause dura mater damage and bone tissue injury [11]. Constructing an accurate mathematical model is difficult due to the irregular lower surface of the skull [12]. Therefore, a pure data-driven model-free adaptive control method based on partial form dynamic linearization is adopted for this process.

According to [13], the multiple-input single-output dynamic linearization data model can be expressed as:

$$\Delta y(k+1) = \boldsymbol{\phi}_L^T(k)\Delta \boldsymbol{U}_L(k) \tag{1}$$

where $\boldsymbol{\phi}_L(k) = [\phi_1(k), \cdots, \phi_L(k)]^T$ is a bounded pseudo gradient vector. $\Delta \boldsymbol{U}_L(k) = [\Delta u(k), \cdots, \Delta u(k-L+1)]^T$. $u(k)$ and $y(k)$ denote the input and output, $\Delta u(k)$ and $\Delta y(k)$ represent the variation in input and output between adjacent time instances. $L$ is called the control input linearization level constant.

Consider the following cost function of control input:

$$J(u(k)) = |y^*(k+1) - y(k+1)|^2 + \lambda \|u(k) - u(k-1)\|^2 \tag{2}$$

where $\lambda > 0$ is a weight factor and $y^*(k+1)$ is the desired output signal. Substituting (1) into (2), and minimizing (2) with respect to $u(k)$ yields the following controller:

$$\begin{aligned} u(k) =& u(k-1) + \frac{\rho_1 \phi_1(k)\left(y^*(k+1) - y(k)\right)}{\lambda + |\phi_1(k)|^2} \\ & - \frac{\phi_1(k)\sum_{i=2}^{L} \rho_i \phi_i(k) \Delta u(k-i+1)}{\lambda + |\phi_1(k)|^2} \end{aligned} \tag{3}$$

where the step factors $\rho_i \in (0, 1], i = 1, 2, \cdots, L$, are added to make the controller algorithm more flexible.

The controller law represented in (3) requires the measured system output $y(k)$, desired force $y^*(k)$, and the time-varying pseudo gradient vector $\boldsymbol{\phi}_L(k)$ in its structure. However, since the pseudo gradient vector is still unknown, the controller algorithm (3) is not adaptable at this stage. Therefore, it is essential to devise a fitting parameter estimation algorithm capable of capturing the time-varying characteristics of pseudo-gradient parameters. The following novel cost function that utilizes the input-output closed-loop data of the controlled plant is considered:

$$\begin{aligned} J(\boldsymbol{\phi}_L(k)) =& \left|y(k) - y(k-1) - \boldsymbol{\phi}_L^T(k)\Delta \boldsymbol{U}_L(k-1)\right|^2 \\ & + \mu \left\|\boldsymbol{\phi}_L(k) - \hat{\boldsymbol{\phi}}_L(k-1)\right\|^2 \end{aligned} \tag{4}$$

where $\mu > 0$ is the weight factor and $\hat{\boldsymbol{\phi}}_L(k)$ is the estimation value of $\boldsymbol{\phi}_L(k)$. Minimizing the cost function (4) with

respect to $\boldsymbol{\phi}_L(k)$, and using matrix inverse lemma [14], the following pseudo gradient vector estimation algorithm is derived:

$$\begin{aligned}\hat{\boldsymbol{\phi}}_L(k) =&\hat{\boldsymbol{\phi}}_L(k-1) + \frac{\eta \Delta \boldsymbol{U}_L(k-1)}{\mu + \|\Delta \boldsymbol{U}_L(k-1)\|^2} \\ &\cdot [y(k) - y(k-1) - \hat{\boldsymbol{\phi}}_L^T(k-1)\Delta \boldsymbol{U}_L(k-1)]\end{aligned} \tag{5}$$

where $\eta \in (0, 2]$ is a step factor. If $\left\|\hat{\boldsymbol{\phi}}_L(k)\right\| \leq \varepsilon$ or $\|\Delta \boldsymbol{U}_L(k-1)\| \leq \varepsilon$ or $\operatorname{sign}(\hat{\phi}_1(k)) \neq \operatorname{sign}(\hat{\phi}_1(1))$, then

$$\hat{\boldsymbol{\phi}}_L(k) = \hat{\boldsymbol{\phi}}_L(1) \tag{6}$$

where $\varepsilon$ represents a small positive constant and $\hat{\boldsymbol{\phi}}_L(1)$ represents the initial value of $\hat{\boldsymbol{\phi}}_L(k)$. A reset mechanism (6) is used to make the parameter estimation algorithm (5) have a stronger ability to track time-varying parameters. When the estimated value of the pseudo gradient vector has been obtained, the controller (3) can be rewritten as:

$$\begin{aligned}u(k) =&u(k-1) + \frac{\rho_1 \hat{\phi}_1(k)\left(y^*(k+1) - y(k)\right)}{\lambda + \left|\hat{\phi}_1(k)\right|^2} \\ &- \frac{\hat{\phi}_1(k)\sum_{i=2}^{L} \rho_i \hat{\phi}_i(k) \Delta u(k-i+1)}{\lambda + \left|\hat{\phi}_1(k)\right|^2}\end{aligned} \tag{7}$$

The pseudo gradient vector estimation algorithms (5), (6), and controller (7) consist of a model-free adaptive control method based on partial form dynamic linearization, and its stability analysis is detailed in [13]. The inputs of this method include the feed force error $\mathbf{F}_{feed\_e}$, the feed force error change $\Delta \mathbf{F}_{feed\_e}$, and the feed displacement change $\Delta l_{feed}$. The output is the feed displacement $l_{feed}$. As the experiment progresses, the controller adjusts the parameters $\hat{\boldsymbol{\phi}}_L(k)$ using (5) according to the changes in the inputs and output. These adjusted parameters are used to regulate the feed displacement $l_{feed}$ for the next time step of the system, which controls the robot's movement in the feed direction, allowing it to adapt to variations in skull thickness and control the feed force within a certain range. The parameters related to weight factors $\lambda$ and $\mu$, step factors $\eta$ and $\rho_i$ are fixed in their specified intervals, and these parameters are chosen by a trial and error method.

### *B. Control Scheme Design*

As shown by the light blue arrow in Fig. 1, the vertical force will cause elastic deformation of the milling cutter protective sheath when milling skulls. In fact, the skull also undergoes slight deformation, but the milling cutter protective sheath is more prone to deformation due to its J-shaped structure [15]. Therefore, the skull is considered a rigid body, and the J-shaped structure of the milling cutter protective sheath is regarded as a spring, with their interaction force considered as the elastic deformation of the milling cutter protective sheath. According to Hooke's Law, the tensile force is expressed as:

$$F_{vertical} = k_c \cdot z \tag{8}$$

where $F_{vertical}$ represents the vertical force, and $k_c$ represents the elastic coefficient, which is an uncertain term. $z$ is the deformation of the milling cutter protective sheath. Since the milling cutter protective sheath is not a standard spring, the elastic coefficient is considered a function of the deformation. Liu proposed a robotic dynamic model to control the contact force between the robot and the unknown environment [16]. Furthermore, controlling the vertical force only requires control along the axis of the milling cutter. Therefore, the dynamics model of the robotic manipulator can be represented:

$$M_d^{'}(\ddot{z}_d - \ddot{z}_t) + D_d^{'}(\dot{z}_d - \dot{z}_t) + K_d^{'}(z_d - z_t) = F_{vertical\_d} - F_{vertical} \tag{9}$$

where $M_d^{'}$, $D_d^{'}$, and $K_d^{'}$ represent the inertia coefficient, damping coefficient, and stiffness coefficient of the manipulator in the vertical direction. $z_d$ and $z_t$ represent the desired and actual vertical positions of the manipulator. $F_{vertical\_d}$ and $F_{vertical}$ represent the desired and actual vertical force. During skull milling, the vertical acceleration of the milling cutter is relatively small, and the quadratic acceleration terms can be neglected. Therefore, (9) can be rewritten as:

$$D_d^{'}(\dot{z}_d - \dot{z}_t) + K_d^{'}(z_d - z_t) = F_{vertical\_d} - F_{vertical} \tag{10}$$

The vertical force error between the desired and actual value of the milling cutter protective sheath is denoted as:

$$E = F_{vertical\_d} - F_{vertical} \tag{11}$$

Combining (8), (10), and (11), (12) is obtained:

$$\frac{D_d^{'}}{k_c}\dot{E} + \left(\frac{K_d^{'}}{k_c} - 1\right)E = 0 \tag{12}$$

(12) indicates that by employing a PD controller, the force of the milling cutter protective sheath in the vertical direction can be controlled. However, (12) includes the error's and its derivative's coefficients, denoted as $D_d^{'}$ and $K_d^{'}$, which vary with time, and an uncertain term $k_c$. To address such issues of model uncertainty and time variation, fuzzy control is commonly adopted in engineering. Moreover, compared to a PD controller, adding an integral term can decrease steady-state errors. Therefore, fuzzy PID control and model-free adaptive control method based on partial form dynamic linearization are combined to control the milling cutter's vertical and feed force within a certain range.

The fuzzy controller is designed with two inputs and one output and employs a conventional two-dimensional control structure. The inputs of the controller are $\mathbf{F}_{total\_e}$ and $\Delta \mathbf{F}_{total\_e}$. $\mathbf{F}_{total\_e}$ is the sum of the feed force error $\mathbf{F}_{feed\_e}$ and the vertical force error $\mathbf{F}_{vertical\_e}$, and $\Delta \mathbf{F}_{total\_e}$ is the total error change between two adjacent sampling intervals. The controller's output is the vertical displacement $l_{vertical}$.

Fuzzification transforms the input and output variables into fuzzy quantities. Gaussian functions are employed as membership functions to define the mapping of inputs to membership values within the range of 0 to 1. Within

TABLE I

THE RULE BASE FOR THE FUZZY PID CONTROLLER

| $\Delta k_p/\Delta k_i/\Delta k_d$ | | $\Delta \mathbf{F}_{total\_e}$ | | | | |
|---|---|---|---|---|---|---|
| | | NB | NS | ZO | PS | PB |
| $\mathbf{F}_{total\_e}$ | NB | PB/NB/NS | PB/NB/ZO | PB/NS/NB | PB/NS/NB | ZO/ZO/NS |
| | NS | PB/ZO/NS | PB/NS/NB | PS/NS/NB | ZO/ZO/NS | PS/PS/NS |
| | ZO | NB/NS/ZO | PS/NS/NS | ZO/ZO/NS | NS/PS/NS | NS/PB/NS |
| | PS | PS/NS/ZO | ZO/ZO/ZO | NS/PS/ZO | NB/PS/ZO | NB/PB/ZO |
| | PB | ZO/ZO/PS | NS/PS/PS | NB/NB/PS | NB/PS/PB | NB/PB/PS |

the domain of the fuzzy controller, the inputs $\mathbf{F}_{total\_e}$, $\Delta\mathbf{F}_{total\_e}$, and output $l_{vertical}$ are denoted by:

$$\mathbf{F}_{total\_e},\ \Delta\mathbf{F}_{total\_e},\ l_{vertical} = \{\mathbf{x} : x \in [-2, 2] \text{ and } x \in \mathbf{Z}\} \tag{13}$$

The corresponding fuzzy quantities are defined for the rule base as negative big (NB), negative small (NS), zero (ZO), positive small (PS), and positive big (PB), whose rules are shown in Table I. Table I summarizes most cases and the corresponding control strategies, and the experience is described by experts and verified by data collection. The scaling factor $k$ can establish a quantitative relationship between the actual value and the domain of the fuzzy controller. If the error has a range of $[e_L, e_H]$, the scaling factor can be defined using the following equation:

$$k = \frac{4}{e_H - e_L} \tag{14}$$

According to the rules outlined in Table I, the output can be derived through the process of defuzzification. By mapping the actual error and the error change rate and referring to Table I in real-time, PID parameters can be adjusted:

$$\begin{cases} k_{p-dynamic} = k_{p-initial} + \Delta k_p \\ k_{i-dynamic} = k_{i-initial} + \Delta k_i \\ k_{d-dynamic} = k_{d-initial} + \Delta k_d \end{cases} \tag{15}$$

where $k_{p-dynamic}$ and $k_{p-initial}$ represent the dynamic and initial proportional coefficient, and $\Delta k_p$ represents the increment of the proportional coefficient under the current circumstances. The adjustment of integral and derivative coefficients follows the same principle.

The admittance controller limits force to prevent excessive force from damaging bone tissue:

$$v_{feed} = \begin{cases} 0, & \text{if} \quad |\mathbf{F}_t| > |\mathbf{F}_{th}| \\ V_{ref} + K_f \cdot (\mathbf{F}_{desired} - \mathbf{F}_t) \ - K_d \cdot v_{feed}, & \text{otherwise} \end{cases} \tag{16}$$

where $v_{feed}$ and $V_{ref}$ are the milling cutter's feed velocity and reference feed velocity. $K_f$ and $K_d$ are the coefficients, and $\mathbf{F}_{desired}$ is the desired force. $\mathbf{F}_t$ is the real-time force and $\mathbf{F}_{th}$ is the force threshold, ensuring that the force does not exceed the manipulator's load. The robot controller can be expressed as:

$$\dot{q} = J^{\dagger}(q)(\dot{p}_d + K_p \cdot p_{offset}) \tag{17}$$

where $q$ is defined as the joint space vector, $J^{\dagger}(q)$ is the pseudo-inverse of the Jacobian matrix $J(q)$, $p_{offset}$ represents the task space offset vector, and $K_p$ is a symmetric positive matrix. $p_d$ is the desired task space vector.

The control block diagram is shown in Fig. 2.

## IV. EXPERIMENTS

### A. Robot System Construction

This robot-assisted cranial milling system has been improved based on our previous work [17]. The main difference is that the previous work focused on robot-assisted cranial drilling, while the current task is cranial milling. The system consists of a 7-DOF robot system (Agile robots, China), a skull-milling dynamic system (B.Braun, China), and a 6-DOF force/torque sensing system (Accuracy 1/16 N, NBIT Inc., China). The skull-milling dynamic system is composed of a milling cutter shank (MCS), an MCS control box, and a pedal switch, all of which are responsible for the skull-milling process. The force sensing system includes a 6-DOF force/torque sensor and a data collector that continuously monitors and feeds back force signals to the controller. In addition, the robot-assisted milling system includes a host computer and an industrial Ethernet switch.

The craniotomy procedure is overseen by a supervisor who can halt it immediately by interrupting the control program or pressing an emergency switch. During the craniotomy process, the supervisor is expected to maintain full pressure on the pedal switch to ensure that the milling cutter operates at its maximum revolutions per minute (rpm).

### B. Experimental Setup

To evaluate the robotic system's suitability for cranial milling, ex vivo animal experiments are conducted using animal skulls obtained from a local slaughter. The programs are developed on Ubuntu 20.04, utilizing the Noetic version of the Robot Operating System (ROS). The skulls from various animals exhibit different thicknesses, with goat skulls ranging from 6 mm to 20 mm, dog skulls from 4 mm to 7 mm, and human skulls from 4 mm to 14 mm [18]. As the milling trajectory is relatively short and the experiment is performed at the top of the skull, it is assumed that the milling cutter and the skull maintain an approximate vertical alignment throughout the process. In this experiment, the desired vertical force for the milling cutter is set to $\mathbf{F}_{vertical\_d} = 2.0$ N, which meets the requirements of clinical surgery [19]. [20] indicates that excessive feed force can damage normal bone tissue or break the milling cutter, and it is constrained to $\mathbf{F}_{feed\_th} = 30.0$ N [21]. Moreover, considering the elastic modulus of the dura mater, which is approximately 70±44 MPa [22], and multiplying it by the contact area at the end of the milling cutter shank, the maximum force the dura mater can withstand is estimated to be around 6.24 N. Consequently, the threshold for vertical force is set to $\mathbf{F}_{vertical\_th} = -6.0$ N. The maximum spindle velocity of the milling cutter is $v_{spindle} = 80,000$ rpm, and the reference feed velocity of the milling cutter is set to $V_{ref} = 0.1$ mm/s or $0.2$ mm/s. The force sensor's sampling frequency is set to $f_{sensor} = 200$ Hz. The experimental scenario is depicted in Fig. 3.

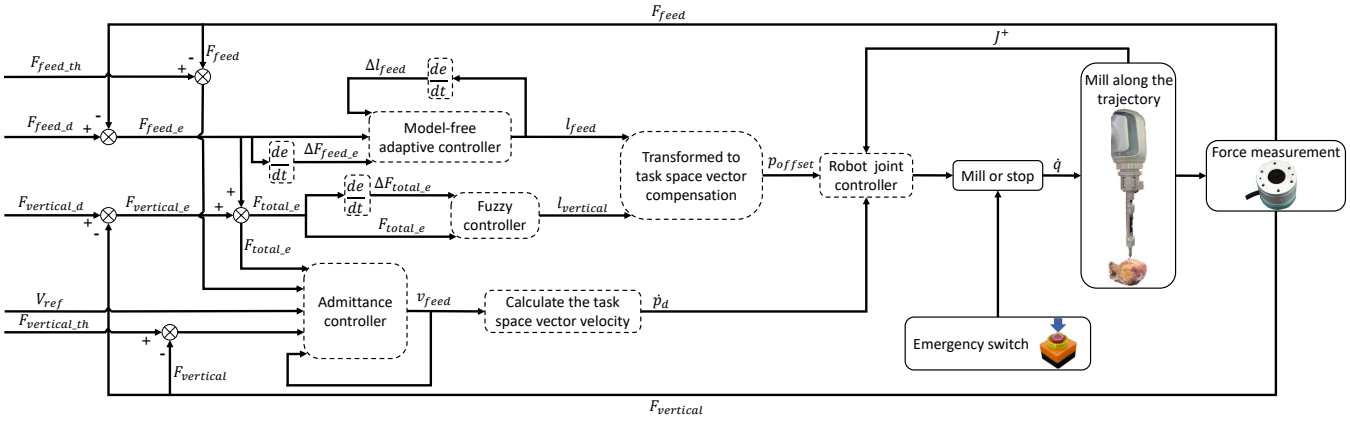


Fig. 2. A robotic skull-milling system's control block diagram. The milling cutter's maximum reference feed velocity is set to 0.2 mm/s, with a feed force limited to 30.0 N. The milling process can be interrupted by the supervisor when an emergency occurs.

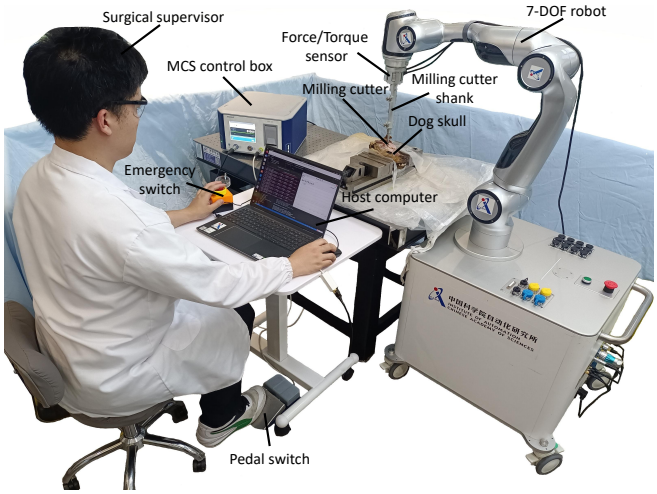


Fig. 3. Automatic robotic skull-milling experiment scene. A supervisor would continuously monitor the milling process, with the ability to halt the operation if necessary.

### C. Validation of Hybrid Admittance Control Algorithm

At first, the milling cutter's position and posture are manually adjusted and inserted into the hole. Subsequently, the milling cutter's posture is fine-tuned to ensure its perpendicular alignment with the skull. Nevertheless, owing to the inherent randomness of manual adjustments, the initial force varies. When performing the dog skull-milling experiments at $V_{ref} = 0.1$ mm/s or 0.2 mm/s, according to [10], the desired feed forces are about $F_{feed\_d} = 5.0$ N and 10.0 N, respectively. The desired feed forces are about $F_{feed\_d} = 10.0$ N and 15.0 N in the goat skull-milling experiments due to the thicker goat skull. As the skull exerts a force in the opposite direction of the milling cutter's feed direction, the feed force is negative. The PID control method and the proposed hybrid admittance control algorithm are used to conduct the experiments. Based on multiple experiments, the parameter settings for the PID controller are shown in Table II. The experimental results are shown in Fig. 4, Table III and Table IV. Fig. 5 provides a direct representation

TABLE II

PID CONTROLLER PARAMETERS

| Parameter | Value |
|---|---|
| Proportional gain | 0.8 |
| Integral gain | 0.3 |
| Derivative gain | 0.2 |

TABLE III

ROOT MEAN SQUARE VERTICAL FORCE ERRORS

| Method | Sample | Reference velocity | Force error | Error percentage |
|---|---|---|---|---|
| Proposed method | $dog_1$ | 0.1 mm/s | 0.037 N | 1.85% |
| | $dog_2$ | 0.2 mm/s | 0.022 N | 1.10% |
| | $goat_1$ | 0.1 mm/s | 0.011 N | 0.55% |
| | $goat_2$ | 0.2 mm/s | 0.021 N | 1.05% |
| PID control | $dog_1$ | 0.1 mm/s | 0.402 N | 20.10% |
| | $dog_2$ | 0.2 mm/s | 0.207 N | 10.35% |
| | $goat_1$ | 0.1 mm/s | 0.226 N | 11.30% |
| | $goat_2$ | 0.2 mm/s | 0.196 N | 9.80% |

of the force applied to the animal skulls under different reference feed velocities of the milling cutter when using the proposed method. Fig. 6 shows images of the skulls after the experiments.

## V. DISCUSSION

A total of 42 cranial milling experiments are conducted, with no instance of dura mater damage observed. The success rate of dura mater protection reaches 100.0%, significantly higher than that of traditional cranial surgeries where dura mater damage occurs in approximately 30% of cases [23], and superior to the performance of previous research where the dura mater protection success rate is 94.08% [24]. Additionally, the robot demonstrates a higher level of autonomy, as it only requires a supervisor to operate the pedal switch, while all other tasks are automatically performed by the robot. This level of autonomy surpasses that of previous research where surgeons perform craniotomy procedures using master-slave manipulation or by manually assisting the robot [6], [25], [26].

Fig. 4 demonstrates that the proposed control algorithm can maintain force error below 5.0% within 3 s, which meets

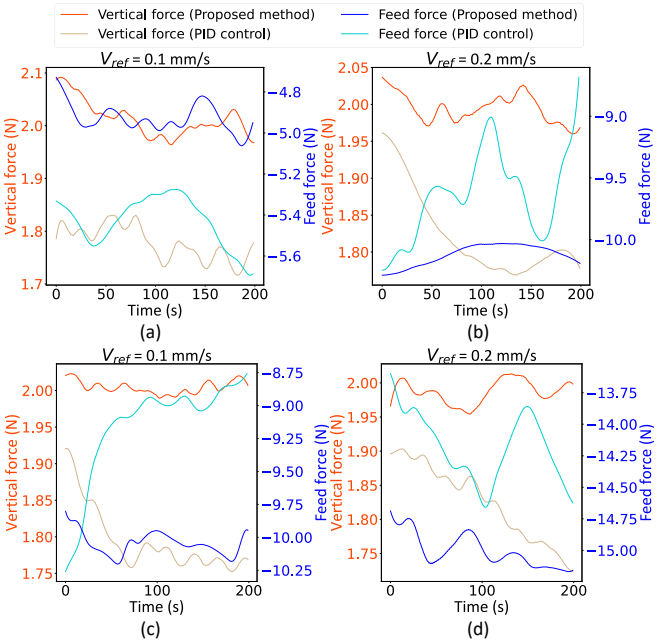


Fig. 4. Experimental data of vertical and feed forces in robotic skull milling. Subfigures (a) and (b) show the experimental results for the dog skull milling. Subfigures (c) and (d) show the experimental results for the goat skull milling. The orange and blue lines represent the force data in the vertical and feed directions using the proposed method. The tan and green lines indicate the force data in the vertical and feed directions using the PID control method.

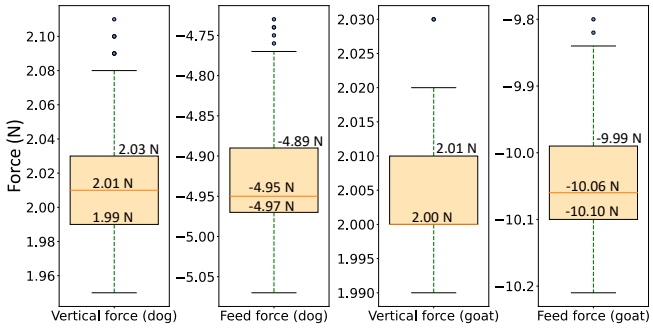


(a) Force analysis at the reference feed velocity of 0.1 mm/s

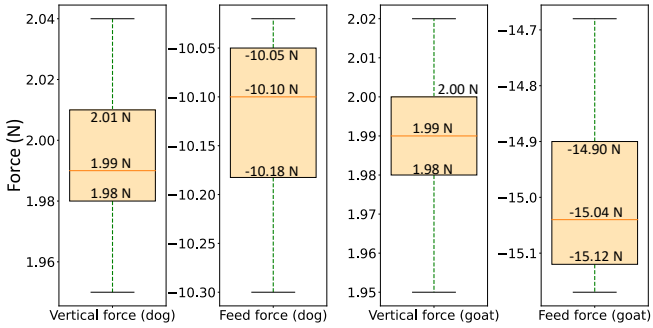


(b) Force analysis at the reference feed velocity of 0.2 mm/s

Fig. 5. Box plot of skull milling experimental data at different reference feed velocities when using the proposed method. Subfigures (a) and (b) illustrate the vertical and feed forces applied to the animal skulls by the milling cutter at reference feed velocities of 0.1 mm/s and 0.2 mm/s, respectively.

bone-milling clinical surgery's requirements [27] and outperforms other methods where the force control's stability time

TABLE IV

ROOT MEAN SQUARE FEED FORCE ERRORS

| Method | Sample | Reference velocity | Force error | Error percentage |
|---|---|---|---|---|
| Proposed method | $dog_3$ | 0.1 mm/s | 0.097 N | 1.94% |
| | $dog_4$ | 0.2 mm/s | 0.147 N | 1.47% |
| | $goat_3$ | 0.1 mm/s | 0.099 N | 0.99% |
| | $goat_4$ | 0.2 mm/s | 0.133 N | 0.89% |
| PID control | $dog_3$ | 0.1 mm/s | 0.476 N | 9.52% |
| | $dog_4$ | 0.2 mm/s | 0.833 N | 8.33% |
| | $goat_3$ | 0.1 mm/s | 1.033 N | 10.33% |
| | $goat_4$ | 0.2 mm/s | 1.153 N | 7.68% |

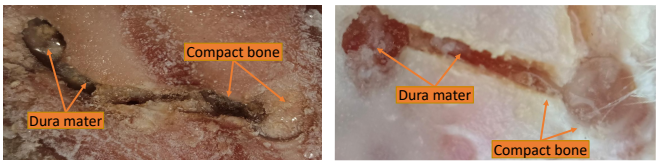


(a) (b)

Fig. 6. The images of the cranium after the skull-milling experiments. Subfigures (a) and (b) show the cranium after the milling experiments on the dog and goat skulls.

exceeds 10 s [28], [29]. Fig. 5 demonstrates that as the feed velocity increases, the milling cutter's oscillation becomes more severe. However, the majority of the error percentage remains within 2.0%. Table III and Table IV demonstrate that the proposed control methods exhibit significantly superior performance compared to the PID control algorithm. Fig. 6 illustrates that the dura mater remains intact after the skull-milling process. Overall, the control scheme and developed system increase the autonomy level of the craniotomy robot, and the results of force control experiments are superior to those obtained with previous mainstream methods where the force error percentages are over 8.0% [11], [30], [31].

The experimental results reveal two areas for improvement in the system. First, the manipulator's pose accuracy needs improvement. Second, significant jitters occur during the skull milling process, and it is speculated that the milling cutter may encounter rigid bone structures. In the future, the integration of real-time navigation into the craniotomy procedure can enhance the precision of force and pose.

## VI. CONCLUSION

A hybrid admittance control algorithm combining a model-free adaptive nonlinear force control and fuzzy control algorithms is proposed to effectively execute automated cranial milling tasks. 42 ex vivo animal skull-milling experiments conducted by the automatic robotic cranium-milling system demonstrate that the proposed algorithm maintains force error percentages below 5.0% within 3 s, with maximal root mean square error percentages for vertical and feed forces at 1.85% and 1.94%, respectively. Moreover, no instances of dura mater damage are observed and the robotic system shows a high level of autonomy. The results provide a potential to enhance the intelligence level of neurosurgery in the future. Future work will incorporate a real-time navigation system to further enhance its applicability in clinical settings.

## REFERENCES


[1] S. Tharin and A. Golby, "Functional brain mapping and its applications to neurosurgery," *Operative Neurosurgery*, vol. 60, no. suppl_4, pp. ONS–185, 2007.

[2] D. Teichmann, L. Rohé, A. Niesche, M. Mueller, K. Radermacher, and S. Leonhardt, "Estimation of penetrated bone layers during craniotomy via bioimpedance measurement," *IEEE Transactions on Biomedical Engineering*, vol. 64, no. 4, pp. 765–774, 2016.

[3] Q. H. Li, L. Zamorano, A. Pandya, R. Perez, J. Gong, and F. Diaz, "The application accuracy of the neuromate robot—a quantitative comparison with frameless and frame-based surgical localization systems," *Computer Aided Surgery*, vol. 7, no. 2, pp. 90–98, 2002.

[4] L. Zamorano, Q. Li, S. Jain, and G. Kaur, "Robotics in neurosurgery: state of the art and future technological challenges," *Int J Med Robot*, vol. 1, no. 1, pp. 7–22, 2004.

[5] M. J. Lang, A. D. Greer, and G. R. Sutherland, *Intra-operative robotics: NeuroArm*. Springer, 2011.

[6] C. Xu, L. Lin, Z. Mar Aung, G. Chai, and L. Xie, "Research on spatial motion safety constraints and cooperative control of robot-assisted craniotomy: Beagle model experiment verification," *The International Journal of Medical Robotics and Computer Assisted Surgery*, vol. 17, no. 2, p. e2231, 2021.

[7] Z. Deng, H. Jin, Y. Hu, Y. He, P. Zhang, W. Tian, and J. Zhang, "Fuzzy force control and state detection in vertebral lamina milling," *Mechatronics*, vol. 35, pp. 1–10, 2016.

[8] D. Wu, L. Zhang, and S. Liu, "Research on establishment and validation of cutting force prediction model for bone milling," in *2015 IEEE International Conference on Robotics and Biomimetics (ROBIO)*, pp. 1864–1869, IEEE, 2015.

[9] K. I. A.-l. Al-Abdullah, H. Abdi, C. P. Lim, and W. A. Yassin, "Force and temperature modelling of bone milling using artificial neural networks," *Measurement*, vol. 116, pp. 25–37, 2018.

[10] Q. Zheng, Y. Lin, X. Chen, L. He, C. Zhang, Y. Hu, and W. Fu, "Optimization of cranial bone milling parameters'in craniotomy: A milling force model and its experimental validation," *Journal of Mechanics in Medicine and Biology*, vol. 22, no. 07, p. 2250059, 2022.

[11] M. Li, X. Qi, Y. Sun, B. Li, Y. Hu, and W. Tian, "A stability and safety control method in robot-assisted decompressive laminectomy considering respiration and deformation of spine," *IEEE Transactions on Automation Science and Engineering*, 2022.

[12] H. Preuschoft and U. Witzel, "Functional shape of the skull in vertebrates: which forces determine skull morphology in lower primates and ancestral synapsids?," *The Anatomical Record Part A: Discoveries in Molecular, Cellular, and Evolutionary Biology: An Official Publication of the American Association of Anatomists*, vol. 283, no. 2, pp. 402–413, 2005.

[13] Z. Hou and Y. Zhu, "Controller-dynamic-linearization-based model free adaptive control for discrete-time nonlinear systems," *IEEE Transactions on Industrial Informatics*, vol. 9, no. 4, pp. 2301–2309, 2013.

[14] G. C. Goodwin and K. S. Sin, *Adaptive filtering prediction and control*. Courier Corporation, 2014.

[15] Y. Ma, X. Feng, J. A. Rogers, Y. Huang, and Y. Zhang, "Design and application of 'j-shaped'stress–strain behavior in stretchable electronics: a review," *Lab on a Chip*, vol. 17, no. 10, pp. 1689–1704, 2017.

[16] H. Liu, L. Wang, and F. Wang, "Fuzzy force control of constrained robot manipulators based on impedance model in an unknown environment," *Frontiers of Mechanical Engineering in China*, vol. 2, pp. 168–174, 2007.

[17] G.-B. Bian, B.-T. Wei, Z. Li, P. Ge, Z. Chen, C. Qian, J. Wang, P. Fu, and J. Zhao, "Robotic automatic drilling for craniotomy: Algorithms and in vitro animal experiments," *IEEE/ASME Transactions on Mechatronics*, 2023.

[18] H. Mahinda and O. P. Murty, "Variability in thickness of human skull bones and sternum–an autopsy experience," *Journal of Forensic Medicine and Toxicology*, vol. 26, no. 2, pp. 26–31, 2009.

[19] M. Hollensteiner, D. Fürst, B. Esterer, P. Augat, F. Schrödl, S. Hunger, M. Malek, D. Stephan, and A. Schrempf, "Novel bone surrogates for cranial surgery training," *Journal of the Mechanical Behavior of Biomedical Materials*, vol. 72, pp. 49–51, 2017.

[20] R. K. Pandey and S. Panda, "Drilling of bone: A comprehensive review," *Journal of clinical orthopaedics and trauma*, vol. 4, no. 1, pp. 15–30, 2013.

[21] H. Huiyu, W. Chengyong, Z. Yue, Z. Yanbin, X. Linlin, X. Guoneng, Z. Danna, C. Bin, and C. Haoan, "Investigating bone chip formation in craniotomy," *Proceedings of the Institution of Mechanical Engineers, Part H: Journal of Engineering in Medicine*, vol. 231, no. 10, pp. 959–974, 2017.

[22] J. Zwirner, M. Scholze, J. N. Waddell, B. Ondruschka, and N. Hammer, "Mechanical properties of human dura mater in tension–an analysis at an age range of 2 to 94 years," *Scientific reports*, vol. 9, no. 1, pp. 1–11, 2019.

[23] D. Han, X. Duan, M. Li, T. Cui, A. Ma, and X. Ma, "Interaction control for manipulator with compliant end-effector based on hybrid position-force control," in *2017 IEEE International Conference on Mechatronics and Automation (ICMA)*, pp. 863–868, IEEE, 2017.

[24] L. Xingzhou, Z. Ziwei, Y. Yingjie, C. Xiaojun, and Z. Yan, "Novel man-machine cooperative robot-assisted craniotomy: A pilot animal experiment on feasibility and safety," *Journal of Tissue Engineering and Reconstructive Surgery*, vol. 18, no. 4, p. 289, 2022.

[25] X. Duan, H. Tian, C. Li, Z. Han, T. Cui, Q. Shi, H. Wen, and J. Wang, "Virtual-fixture based drilling control for robot-assisted craniotomy: Learning from demonstration," *IEEE Robotics and Automation Letters*, vol. 6, no. 2, pp. 2327–2334, 2021.

[26] T. Essomba, J. Sandoval, M. A. Laribi, C.-T. Wu, C. Breque, S. Zeghloul, and J.-P. Richer, "Kinematic and force experiments on cadavers for the specification of a tele-operated craniotomy robot," in *Advances in Service and Industrial Robotics: Proceedings of the 28th International Conference on Robotics in Alpe-Adria-Danube Region (RAAD 2019) 28*, pp. 447–454, Springer, 2020.

[27] N. Sugita, T. Nakano, Y. Nakajima, K. Fujiwara, N. Abe, T. Ozaki, M. Suzuki, and M. Mitsuishi, "Dynamic controlled milling process for bone machining," *Journal of Materials Processing Technology*, vol. 209, no. 17, pp. 5777–5784, 2009.

[28] D. Xu, X. Shen, Z. Mo, and Y. Fan, "Empirical formula and experiment based force modeling for haptic spine surgery simulation," *International Journal of Modeling, Simulation, and Scientific Computing*, vol. 2, no. 01, pp. 29–44, 2011.

[29] H. Qu, B. Geng, B. Chen, J. Zhang, Y. Yang, L. Hu, and Y. Zhao, "Force perception and bone recognition of vertebral lamina milling by robot-assisted ultrasonic bone scalpel based on backpropagation neural network," *Ieee Access*, vol. 9, pp. 52101–52112, 2021.

[30] Q.-S. Chen, L. Dai, Y. Liu, and Q.-X. Shi, "A cortical bone milling force model based on orthogonal cutting distribution method," *Advances in Manufacturing*, vol. 8, pp. 204–215, 2020.

[31] G. Pei, M. Yu, Y. Xu, C. Ma, H. Lai, F. Chen, and H. Lin, "An improved pid controller for the compliant constant-force actuator based on bp neural network and smith predictor," *Applied Sciences*, vol. 11, no. 6, p. 2685, 2021.